MuSR METHOD AND TOMOGRAPHIC PROBABILITY REPRESENTATION OF SPIN STATES

Yu. M. Belousov[1], S. N. Filippov[1*], V. N. Gorelkin[1], and V. I. Man'ko[2]

[1] *Moscow Institute of Physics and Technology (State University)*
Institutskii per. 9, Dolgoprudnyi, Moscow Region 141700, Russia

[2] *P. N. Lebedev Physical Institute, Russian Academy of Sciences*
Leninskii Prospect 53, Moscow 119991, Russia

*Corresponding author, e-mail: sergey.filippov@phystech.edu
e-mail: theorphys@phystech.edu, gorelkin2004@mail.ru, manko@sci.lebedev.ru

Abstract

Muon spin rotation/relaxation/resonance (MuSR) technique for studying matter structures is considered by means of a recently introduced probability representation of quantum spin states. A relation between experimental MuSR histograms and muon spin tomograms is established. Time evolution of muonium, anomalous muonium, and a muonium-like system is studied in the tomographic representation. Entanglement phenomenon of a bipartite muon-electron system is investigated via tomographic analogues of Bell number and positive partial transpose (PPT) criterion. Reconstruction of the muon-electron spin state as well as the total spin tomography of composed system is discussed.

Keywords: MuSR method, qubits in solid state structures, entanglement, Bell inequality, PPT criterion, probability representation of quantum mechanics, quantum tomography.

1 Introduction

The description of spin states is usually based on the concept of density matrix. The density matrix formalism was introduced originally by Landau [1] and von Neumann [2] for continuous variables, and then successfully extended to the case of discrete variables and spin states (see, e.g. [3]). In contrast to the state of classical particle, the density matrix cannot be measured immediately in the experiment, as the outcomes of quantum observables have a probabilistic nature. The attempt to bring classical and quantum descriptions closer together was made by Wigner [4], who introduced the quasi-probability function $W(q,p)$ in phase space such that marginal distributions $\int W(q,p)dp$ and $\int W(q,p)dq$ are true probability distribution of position and momentum, respectively. However, Wigner function can take negative values. Moreover, there is no direct way to measure W-function. So far many quasi-probability functions were introduced, for instance, Hisimi Q-function [5] and Sudarshan-Glauber P-function [6, 7] (the review of different quasi-probability distributions is presented in [8]). Experimental needs to reconstruct density matrix or Wigner function of photon states by means of experimentally measured probability distributions resulted in developing tomographic methods (both theoretical [9–11, 18] and experimental [12,13]) based on Radon transform [14,15]. Though tomograms were originally considered as auxiliary tools, recently it was proposed to treat tomograms as primary notions of quantum states [16,17] because a tomogram is a fair probability distribution function, contains the same information about the system as a density matrix, and the crucial fact is that tomograms can be measured in laboratory. The tomographic description of light states was extended to include optical tomography [9, 10], symplectic tomography [11], photon-number tomography [18–20], and their recent generalizations [21, 22]. The tomographic-probability representation was then extended to spin states [23,24] and developed in [25,26]. In the paper [27], the general form of unitary spin tomography was considered. The spin tomography

with a finite number of rotations was discussed in [28]. We refer the reader to the review [29] for detailed history of the tomographic-probability representation.

The aim of this paper is to apply spin tomograms to muon spin rotation/relaxation/resonance experiments usually abbreviated to MuSR or acronym μSR. At present, MuSR method is primarily used to get insight about the microscopic behavior of materials and nanostructures (see the reviews [30–32]), although the origin of this method is due to experimental verification of the proposal that the weak interaction might violate parity symmetry, and measuring the anisotropy of muon decay predicted by V-A theory of weak interactions. Muons (μ) are utilized in μSR technique as probes. Muon is a short-lived subatomic particle and has the following properties: charge ± 1 elementary charge (μ^+ and μ^-, respectively), mass $m_\mu = 206.77\ m_e$, spin $s = 1/2$, magnetic moment $\mu_\mu = 3.18334\ \mu_p$, mean lifetime $\tau = 2.197 \cdot 10^{-6}\ s$. Positive (negative) muon decays into positron (electron) and a neutrino-antineutrino pair as follows:

$$\mu^+ \longrightarrow e^+ + \nu_e + \tilde{\nu}_\mu, \qquad \mu^- \longrightarrow e^- + \tilde{\nu}_e + \nu_\mu. \tag{1}$$

Thanks to violation of parity symmetry, during the decay of μ^+, the positron e^+ is preferentially emitted along the direction of muon spin. The decay positron can be emitted along an arbitrary direction but the probability of such an event depends on the direction $\mathbf{n} = (\cos\varphi \sin\theta, \sin\varphi \sin\theta, \cos\theta)$ (anisotropy). Nevertheless, it is possible to measure the angular distribution $\Gamma(\mathbf{n})$ of the decay positrons from a bunch of muons (ensemble) deposited at the same conditions. If detectors are capable to detect positrons of an arbitrary energy (from 0 to ∞) and muon spin is aligned along the z-axis, i.e. its vector state $|j^{(\mu)} = 1/2, m^{(\mu)} = 1/2\rangle$ is an eigenstate of angular momentum operators $\hat{J}_z$ and $\hat{\mathbf{J}}^2$, then the angular distribution $\Gamma(\mathbf{n})$ reads (see, e.g. [30])

$$\Gamma(\mathbf{n})\frac{d\mathbf{n}}{4\pi} = \left(1 + \frac{1}{3}\cos\theta\right)\frac{\sin\theta d\theta d\varphi}{4\pi}. \tag{2}$$

The corresponding directional diagram is depicted in Fig. 1a. The asymmetry of angular distribution (2) allows to reconstruct the spin state of muon. Moreover, observing the time evolution $\Gamma(\mathbf{n}, t)$ (measuring μSR histograms) allows to trace the time evolution of the muon spin polarization which depends sensitively on the magnetic environment. In this paper, we relate the μSR histogram $\Gamma(\mathbf{n}, t)$ and a spin tomogram $w(m, \mathbf{n}, t)$.

The other aim of this paper is to consider the spin system of muonium Mu $= \mu^+ e^-$ from the tomographic point of view. Muonium is formed in certain materials (for instance, in semiconductors) when a positive muon μ^+ picks up an electron. If this is the case, muonium turns out to be a light isotope of hydrogen and is of interest not only in solid state physics but also in chemistry [33]. Thanks to a hyperfine coupling, the information contained in the electron spin can be passes on to the muon spin which is then analyzed via different μSR techniques. Employing the tomographic-probability representation, we are interested not only in reconstructing density matrix of muon-electron spin state but also in formation, controlling, and detecting entanglement of this system. Such an approach would be useful to realize in practice a challenging idea: check Bell inequalities with the help of true spins states not polarizations of photons.

The paper is organized as follows.

In Sec. 2, we review briefly the tomography of a single spin and derive the relation between the μSR histogram and the qubit tomogram. In Sec. 3, we focus our attention on muonium and muonium-like systems and address the problem of two-spin tomography. In Sec. 4, using the tomographic-probability representation, the entanglement phenomenon, Bell-like inequality, and positive partial transpose are discussed. In Sec. 5, a time evolution of tomograms is considered. In Sec. 6, we address muonium and muonium-like systems in order to introduce their spin Hamiltonian operator. In Sec. 7, the time evolution and entanglement of Mu and Mu-like systems are investigated in the tomographic representation. Also, a method for reconstructing muon-electron spin state is discussed. In Sec. 8, conclusions are presented.

2 Muon Spin Tomography

Any spin-j state given by the density operator $\hat{\rho}$ can be alternatively described by the following unitary spin tomogram $w^{(j)}(m,\hat{u})$ [27]:

$$w^{(j)}(m,\hat{u}) = \langle jm|\hat{u}\hat{\rho}\hat{u}^{\dagger}|jm\rangle, \tag{3}$$

where $|jm\rangle$ is an eigenvector of angular momentum operators $\hat{J}_z$ and $\hat{\mathbf{J}}^2$, m is the spin projection on z-direction ($m=-j,-j+1,\ldots,j$), $\hat{u}$ is a general unitary transformation which is given by $(2j+1)\times(2j+1)$ matrix $u\in SU(N)$, $N=2j+1$ in the basis of states $|jm\rangle$. The inverse mapping $w^{(j)}(m,\hat{u})$ is also developed in [27] and implies integration over all unitary matrices $u\in SU(N)$ via a corresponding measure. We emphasize the unique properties of the unitary spin tomogram (3): non-negativity $w^{(j)}(m,\hat{u})\geq 0$ and normalization $\sum_{m=-j}^{j} w^{(j)}(m,\hat{u})=1$. The physical meaning of the tomogram (3) is the probability to obtain the spin projection m after a unitary rotation $\hat{u}\hat{\rho}\hat{u}^{\dagger}$ of the spin-j state is fulfilled.

For our purposes, it is important to consider the case $u\in SU(2)$, when the unitary spin tomogram transforms into a spin tomogram $w(m,\mathbf{n})$ introduced in [23,24]. Indeed, if this is the case, it is possible to parameterize $\hat{u}=\hat{R}(\mathbf{n})$ by unit vector $\mathbf{n}=(\cos\varphi\sin\theta,\sin\varphi\sin\theta,\cos\theta)$ as follows:

$$\hat{R}(\mathbf{n}) = e^{-i(\mathbf{n}_{\perp}\cdot\,\hat{\mathbf{J}})\theta}, \qquad \mathbf{n}_{\perp}=(-\sin\phi,\cos\phi,0). \tag{4}$$

For example, in case of qubits ($j=1/2$) the matrix of operator (4) in the basis of states $|jm\rangle$ is

$$R(\mathbf{n}) = \begin{pmatrix} \cos(\theta/2) & -\sin(\theta/2)e^{-i\phi} \\ \sin(\theta/2)e^{i\phi} & \cos(\theta/2) \end{pmatrix}. \tag{5}$$

Thus, we obtain the spin tomogram $w(m,\mathbf{n})=\langle jm|\hat{R}(\mathbf{n})\hat{\rho}\hat{R}^{\dagger}(\mathbf{n})|jm\rangle$ which has a sense of probability to obtain m as a result of measuring spin projection on direction $\mathbf{n}$. The inverse mapping of spin tomogram $w^{(j)}(m,\mathbf{n})$ onto the density operator $\hat{\rho}$ reads

$$\hat{\rho} = \sum_{m=-j}^{j} \frac{1}{4\pi} \int_0^{2\pi} d\varphi \int_0^{\pi} \sin\theta d\theta \; w^{(j)}(m,\mathbf{n}(\theta,\varphi))\hat{D}^{(j)}(m,\mathbf{n}(\theta,\varphi)). \tag{6}$$

where $\hat{D}^{(j)}(m,\mathbf{n}(\theta,\varphi))$ is a quantizer operator. According to [23,24], the quantizer operator is expressed through Wigner D-function $D^{(j)}_{m'm}(\alpha,\beta,\gamma)$ as follows:

$$\begin{aligned} \hat{D}^{(j)}(m,\mathbf{n}(\theta,\varphi)) &= (-1)^{m_2'} \sum_{j_3=0}^{2j} \sum_{m_3=-j_3}^{j_3} (2j_3+1)^2 \sum_{m_1,m_1',m_2'=-j}^{j} (-1)^{m_1} D^{(j_3)}_{0m_3}(\theta,\varphi,\gamma) \\ &\times \begin{pmatrix} j & j & j_3 \\ m_1 & -m_1 & 0 \end{pmatrix} \begin{pmatrix} j & j & j_3 \\ m_1' & -m_2' & m_3 \end{pmatrix} |jm_1'\rangle\langle jm_2'|. \end{aligned} \tag{7}$$

We cannot help mentioning that other different forms of the quantizer operator are also known [25,34].

2.1 Tomography of muon spin state

As the tomographic technique is to be applied to muon spin, let us consider the special case $j=1/2$. To avoid confusion, we will denote muon spin $j^{(\mu)}=1/2$ rather than j, muon spin projection $m^{(\mu)}=\pm 1/2$, and angular momentum operators of muon spin are designated by $\hat{\mathbf{J}}^{(\mu)}\equiv(\hat{J}_x^{(\mu)},\hat{J}_y^{(\mu)},\hat{J}_z^{(\mu)})=\frac{1}{2}\hat{\boldsymbol{\sigma}}$, where $\hat{\boldsymbol{\sigma}}\equiv(\hat{\sigma}_x,\hat{\sigma}_y,\hat{\sigma}_z)$ is the set of Pauli operators.

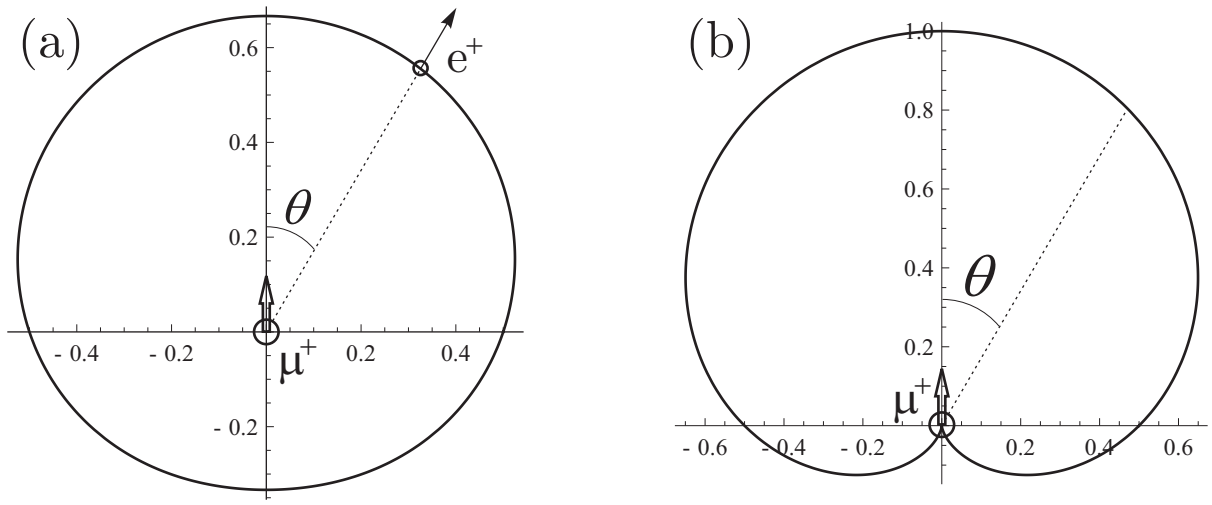

Figure 1: The relation between the angular distribution $\Gamma(\mathbf{n}(\theta,\varphi))$ of positrons e^+ from muon μ^+ decay (a) and the muon spin tomogram $w^{(\mu)}(m^{(\mu)}=+1/2,\mathbf{n}(\theta,\varphi))$ of the state $|\Uparrow\rangle = |j^{(\mu)}=1/2, m^{(\mu)}=1/2\rangle$ (schematically depicted by an arrow).

Using definition (3) and formula (4), it is not hard to see that the spin tomogram of a single muon reads

$$w^{(\mu)}(m^{(\mu)},\mathbf{n}) = \frac{1}{2} + m^{(\mu)}\mathrm{Tr}\big[\hat{\rho}^{(\mu)}\ (\mathbf{n}\cdot\hat{\boldsymbol{\sigma}})\big], \tag{8}$$

whereas the quantizer operator can be written in the following form [25]:

$$\hat{D}^{(\mu)}(m^{(\mu)},\mathbf{n}) = \frac{1}{2}\hat{I} + 3m^{(\mu)}(\mathbf{n}\cdot\hat{\boldsymbol{\sigma}}), \tag{9}$$

with $\hat{I}$ being the identity operator.

In order to compare the muon tomogram $w^{(\mu)}(m^{(\mu)},\mathbf{n})$ and the angular distribution of decay positrons $\Gamma(\mathbf{n})$, let us consider the tomogram of the state $|\Uparrow\rangle \equiv |j^{(\mu)}=1/2, m^{(\mu)}=+1/2\rangle$. Indeed, in this case we obtain

$$\rho^{(\mu)}_{\Uparrow} = \begin{pmatrix} 1 & 0 \\ 0 & 0 \end{pmatrix}, \qquad w^{(\mu)}_{\Uparrow}(+1/2,\mathbf{n}(\theta,\varphi)) = \frac{1}{2}(1+\cos\theta), \qquad w^{(\mu)}_{\Uparrow}(-1/2,\mathbf{n}(\theta,\varphi)) = \frac{1}{2}(1-\cos\theta). \tag{10}$$

The tomogram $w^{(\mu)}_{\Uparrow}(+1/2,\mathbf{n}(\theta,\varphi))$ is depicted in Fig. 1b. Comparing (2) and (10), we derive the following relation between the angular distribution of decay positrons (averaged over all positron energies) and the muon tomogram:

$$w^{(\mu)}(m^{(\mu)}=+1/2,\mathbf{n}) = \frac{3}{2}\Gamma(\mathbf{n}) - 1, \qquad w^{(\mu)}(m^{(\mu)}=-1/2,\mathbf{n}) = 2 - \frac{3}{2}\Gamma(\mathbf{n}). \tag{11}$$

The relations (11) are valid for an arbitrary moment of time t and they give a direct way of transforming μSR histograms into muon spin tomograms $w^{(\mu)}(m^{(\mu)},\mathbf{n},t)$. Moreover, it can be easily checked that the relations (11) are adequate not only for pure states (muon polarization $|\mathbf{P}|=1$) but also for an arbitrary mixed state ($|\mathbf{P}|<1$). As far as negative muons μ^- are concerned, the relation between tomograms and angular distributions of decay electrons is readily obtained by exchanging right-hand sides of Eqs. (11).

In the real experiment, we should take into account the spectral responsivity of positron detectors, and this might result in changing coefficients of relation (11) but linearity of the relation is to be conserved. In

particular, if there were available detectors sensitive only to maximum positron energy $E_{\max} = 52.83$ MeV, it would be possible to measure muon tomogram directly because in this case $w^{(\mu)}(m^{(\mu)} = +1/2, \mathbf{n}) = \Gamma_{E_{\max}}(\mathbf{n})$ and $w^{(\mu)}(m^{(\mu)} = -1/2, \mathbf{n}) = 1 - \Gamma_{E_{\max}}(\mathbf{n})$.

It is known that the muon 2×2 density matrix depends on three real parameters only (vector of polarization $\mathbf{P}$) and can be written in the form $\hat{\rho} = \frac{1}{2}(\hat{I} + (\mathbf{P} \cdot \hat{\boldsymbol{\sigma}}))$. The muon tomogram $w^{(\mu)}(m^{(\mu)}, \mathbf{n})$ is a function on sphere $\mathbf{n} \in S^2$ (and a discrete spin projection). Thus, the muon tomogram contains full and even redundant information about the system. Nevertheless, reconstruction of the density matrix by integration over sphere (see formula (6)) exploits as much experimental information as possible. However, we admit that the practical realization of such an experimental setup (when detectors cover 4π steradian) is a challenge. To eliminate this difficulty one can resort to spin tomography with a finite number of rotations [28]. In case of muons, such a tomography exploits only 3 probabilities $w^{(\mu)}(m^{(\mu)} = +1/2, \mathbf{n}_k)$, $k = 1, 2, 3$. As it is shown in [28], the inverse mapping onto the density operator exists whenever triple product $(\mathbf{n}_1 \cdot [\mathbf{n}_2 \times \mathbf{n}_3]) \neq 0$ and reads

$$\hat{\rho} = \frac{1}{2}\hat{I} + \sum_{k=1}^{3} \Big[2w^{(\mu)}(m^{(\mu)} = +1/2, \mathbf{n}_k) - 1\Big] (\hat{\boldsymbol{\sigma}} \cdot \mathbf{l}_k), \tag{12}$$

where vectors $\mathbf{l}_k$ form a dual basis with respect to directions $\{\mathbf{n}_k\}_{k=1}^3$:

$$\mathbf{l}_1 = \frac{[\mathbf{n}_2 \times \mathbf{n}_3]}{(\mathbf{n}_1 \cdot [\mathbf{n}_2 \times \mathbf{n}_3])}, \quad \mathbf{l}_2 = \frac{[\mathbf{n}_3 \times \mathbf{n}_1]}{(\mathbf{n}_1 \cdot [\mathbf{n}_2 \times \mathbf{n}_3])}, \quad \mathbf{l}_3 = \frac{[\mathbf{n}_1 \times \mathbf{n}_2]}{(\mathbf{n}_1 \cdot [\mathbf{n}_2 \times \mathbf{n}_3])}. \tag{13}$$

It is worth noting that, from experimental point of view, the advantage of formula (12) is that it does not restrict us to using orthogonal directions only. Though if the errors are presented in measured probabilities $w^{(\mu)}(m^{(\mu)} = +1/2, \mathbf{n}_k)$, $k = 1, 2, 3$, the reconstructed density matrix is shown to be the least erroneous when directions $\{\mathbf{n}_k\}_{k=1}^3$ are mutually orthogonal [28]. In up-to-date experiments the background fraction of detector clicks is usually less that 1% of the initial number of counts. At longer timescale $t \gg \tau_\mu$ the background noise does not allow to measure the muon tomogram because the number of muon decays becomes exponentially small.

3 Muonium and Two-Spin Tomography

Dealing with muons, we should not forget their physical implementation and behavior in matter as well as a concrete experimental setup for muon decay investigation. As muons are to be stopped for measuring angular distribution of decay particles, it is important to study behavior of muons in solid state materials. On the other hand, the study of μSR histograms (muon spin tomograms) gives us a useful information about the matter in question. Special attention is paid to the investigation of nanostructures, and this is why we do not consider muons in gases and restrict ourselves to solid state materials.

3.1 Muons in Matter

If negative muon μ^- is incorporated in material, it behaves as a heavy electron and is readily captured by atoms to $1s$ ground state. During its way 'down', muon usually loses the major part of its polarization. In $1s$ state, a space part of the muon wave function is nonzero at an atomic nucleus. This fact may lead to a nuclear capture of the negative muon. As a result, negative muons in matter exhibit relatively small degree of polarization and much shorter lifetime (substantially less than τ_μ). It is the reason why negative muons (μ^-SR technique) are not as often used while investigating local matter properties as positive muons. However, if a negative muon is in $1s$ ground state inside an atom with zero-spin nucleus, the whole system "atom+μ^-" can be regarded as an acceptor center (see, e.g. [35]). The pseudonucleus "nucleus+μ^-" has spin 1/2 and keeps a part of muons initial polarization. For example, negative muons in Si can form ${}^{\mu}Al$ acceptor centers. The effective moment of the electron shell in such centers can take

values greater than 1/2, for example, the case $j^{(e)} = 3/2$ is discussed in the papers [36,37]. Such systems are also of interest for us and we will consider them in Secs. 6.2 and 7.

In contrast, in a condensed matter, positive muons μ^+ are repelled by atomic nuclei and are retarded gradually down to Bohr velocities, and then to thermal velocities within the total time interval $t \sim 10^{-10}$ s. The retarded muon can either come to rest at an interstitial site of high symmetry between the lattice ions (diamagnetic state) or pick up an electron (formation of muonium Mu $= \mu^+ e^-$). A spur model of muonium formation is discussed in [38]. In addition, muon can also become a part of a chemical bound, for instance, with oxygen $O^-\mu^+$ similarly to OH bound. We will focus our attention to muonium. It is worth noting that muonium has almost the same Bohr radius and ionization potential as hydrogen. Also, utilizing ultra-low energy muons (with energies from 0.5 to 30 keV) and selecting their velocities, it is possible to investigate muoniums formed at the implantation depths from less than a nanometer to several hundred nanometers [39, 40]. This fact is crucial for studying surfaces and thin films [41, 42].

Muonium is of special interest for us because it can be considered as a two-spin system. Indeed, averaging over space part of the common wave function, muon spin ($j^{(\mu)} = 1/2$) and electron spin ($j^{(e)} = 1/2$) are coupled by hyperfine interaction $\hat{H}_{\rm hf} = \hbar\omega_0(\hat{\mathbf{J}}^{(\mu)} \odot \hat{\mathbf{J}}^{(e)}) \equiv \hbar\omega_0(\hat{J}_x^{(\mu)} \otimes \hat{J}_x^{(e)} + \hat{J}_y^{(\mu)} \otimes \hat{J}_y^{(e)} + \hat{J}_z^{(\mu)} \otimes \hat{J}_z^{(e)})$, where $\omega_0 = 4453$ MHz.

The aim of the subsequent subsection is to consider two-spin tomography and apply it to the spin state of muonium and muonium-like systems (we will refer to the muon spin 1/2 together with the arbitrary effective electron spin $j^{(e)}$ as Mu-like system).

3.2 Two-Spin Tomography

Let us consider a system comprising two spins: muon spin $j^{(\mu)}$ and an effective electron spin $j^{(e)}$. The state of the system is described by a $N \times N$ density operator $\hat{\rho}$, where $N = (2j^{(\mu)} + 1)(2j^{(e)} + 1)$. If we introduce a basis of system states $\{|i\rangle\}_{i=1}^N$, the density operator can be written in the form of density matrix $\rho_{ij} = \langle i|\hat{\rho}|j\rangle$. There are two common ways to choose basis states:

(i) eigenvectors $|j^{(\mu)}m^{(\mu)}\rangle|j^{(e)}m^{(e)}\rangle$ of individual angular momentum operator $\hat{J}_z^{(\mu)} \otimes \hat{J}_z^{(e)}$;

(ii) eigenvectors $|LM\rangle$ of the total angular momentum operators $\hat{L}_z$ and $\hat{\mathbf{L}}$, where the total spin L can take values $L = |j^{(\mu)} - j^{(e)}|, \ldots, j^{(\mu)} + j^{(e)}$.

Evidently, these two bases are related by the matrix $U_{\rm CG}$ composed of the Clebsch-Gordon coefficients $C^{LM}_{j^{(\mu)}m^{(\mu)}j^{(e)}m^{(e)}} \equiv \langle j^{(\mu)}m^{(\mu)}, j^{(e)}m^{(e)}|LM\rangle$. For muonium ($j^{(\mu)} = 1/2$, $j^{(e)} = 1/2$) the matrix $U_{\rm CG}$ reads

$$\begin{pmatrix} |1,1\rangle \\ |1,0\rangle \\ |1,-1\rangle \\ |0,0\rangle \end{pmatrix} = U_{\rm CG} \begin{pmatrix} |\frac{1}{2},\frac{1}{2}\rangle|\frac{1}{2},\frac{1}{2}\rangle \\ |\frac{1}{2},\frac{1}{2}\rangle|\frac{1}{2},-\frac{1}{2}\rangle \\ |\frac{1}{2},-\frac{1}{2}\rangle|\frac{1}{2},\frac{1}{2}\rangle \\ |\frac{1}{2},-\frac{1}{2}\rangle|\frac{1}{2},-\frac{1}{2}\rangle \end{pmatrix}, \qquad U_{\rm CG} = \begin{pmatrix} 1 & 0 & 0 & 0 \\ 0 & \frac{1}{\sqrt{2}} & \frac{1}{\sqrt{2}} & 0 \\ 0 & 0 & 0 & 1 \\ 0 & \frac{1}{\sqrt{2}} & -\frac{1}{\sqrt{2}} & 0 \end{pmatrix}. \tag{14}$$

Consequently, in the probability representation muonium can be described by two tomograms, namely, an individual two-spin tomogram $w(m^{(\mu)}, \mathbf{n}^{(\mu)}, m^{(e)}\mathbf{n}^{(e)})$ and a total two-spin tomogram $w^{(L)}(M, \mathbf{N})$ discussed below.

3.2.1 Individual Two-Spin Tomogram

Extending the notion of spin tomogram (3) to the case of bipartite spin system, we immediately obtain the individual unitary two-spin tomogram defined through

$$w(m^{(\mu)}, m^{(e)}, \hat{U}) = \langle j^{(\mu)}m^{(\mu)}, j^{(e)}m^{(e)}|\hat{U}\ \hat{\rho}\ \hat{U}^\dagger|j^{(\mu)}m^{(\mu)}, j^{(e)}m^{(e)}\rangle, \tag{15}$$

where $\hat{U}$ is a general $N \times N$ unitary transformation, $N = (2j^{(\mu)} + 1)(2j^{(e)} + 1)$. If $\hat{U}$ is factorized into $\hat{U} = \hat{R}(\mathbf{n}^{(\mu)}) \otimes \hat{R}(\mathbf{n}^{(e)})$, where the rotation operator $\hat{R}$ is given by formula (4), we readily obtain the

so-called individual two-spin tomogram of the form

$$w(m^{(\mu)},\mathbf{n}^{(\mu)},m^{(e)},\mathbf{n}^{(e)})=\langle j^{(\mu)}m^{(\mu)},j^{(e)}m^{(e)}|\hat{R}(\mathbf{n}^{(\mu)})\otimes\hat{R}(\mathbf{n}^{(e)})\ \hat{\rho}\ \hat{R}^{\dagger}(\mathbf{n}^{(\mu)})\otimes\hat{R}^{\dagger}(\mathbf{n}^{(e)})|j^{(\mu)}m^{(\mu)},j^{(e)}m^{(e)}\rangle, \tag{16}$$

which has a clear physical meaning: the individual two-spin tomogram is the joint probability to obtain the value $m^{(\mu)}$ in measuring the muon spin projection on direction $\mathbf{n}^{(\mu)}$ and the value $m^{(e)}$ in measuring the electron spin projection on direction $\mathbf{n}^{(e)}$. Here, measurements are assumed to be simultaneous. Though, in this case, such measurements are not prohibited by quantum mechanics, it is not evident how to realize them in practice. The reconstruction of the density matrix of the whole system is

$$\hat{\rho}=\sum_{m^{(\mu)}=-j^{(\mu)}}^{j^{(\mu)}}\int_{S^2}\frac{d\mathbf{n}^{(\mu)}}{4\pi}\sum_{m^{(e)}=-j^{(e)}}^{j^{(e)}}\int_{S^2}\frac{d\mathbf{n}^{(e)}}{4\pi}\ w(m^{(\mu)},\mathbf{n}^{(\mu)},m^{(e)},\mathbf{n}^{(e)})\hat{D}^{(j^{(\mu)})}(m^{(\mu)},\mathbf{n}^{(\mu)})\otimes\hat{D}^{(j^{(e)})}(m^{(e)},\mathbf{n}^{(e)}), \tag{17}$$

where the local quantizer operator $\hat{D}^{(j)}(m,\mathbf{n})$ is given by formula (7).

As mentioned above, the practical realization of measuring the individual spin-tomogram is a challenge. In the fact, the μSR-method (discussed in Sec. 2) allows measuring the muon part of the tomogram only. Using the probability interpretation of the tomogram (16), we can say that only the following marginal distribution is measurable via μSR technique:

$$\begin{aligned}\widetilde{w}(m^{(\mu)},\mathbf{n}^{(\mu)}) &= \sum_{m^{(e)}=-j^{(e)}}^{j^{(e)}} w(m^{(\mu)},\mathbf{n}^{(\mu)},m^{(e)}\mathbf{n}^{(e)})=\mathrm{Tr}\big[\hat{\rho}\ \hat{R}^{\dagger}(\mathbf{n}^{(\mu)})|j^{(\mu)}m^{(\mu)}\rangle\langle j^{(\mu)}m^{(\mu)}|\hat{R}(\mathbf{n}^{(\mu)})\otimes\hat{I}^{(e)}\big]\\ &= \langle j^{(\mu)}m^{(\mu)}|\hat{R}(\mathbf{n}^{(\mu)})\ \mathrm{Tr}_e[\hat{\rho}]\ \hat{R}^{\dagger}(\mathbf{n}^{(\mu)})|j^{(\mu)}m^{(\mu)}\rangle,\end{aligned} \tag{18}$$

which is nothing else but the muon spin tomogram of the reduced density operator $\mathrm{Tr}_e[\hat{\rho}]$ (trace is taken over electron spin states). Here, we used the following resolution of identity:

$$\hat{I}^{(e)}=\sum_{m^{(e)}=-j^{(e)}}^{j^{(e)}}\hat{R}^{\dagger}(\mathbf{n}^{(e)})|j^{(e)}m^{(e)}\rangle\langle j^{(e)}m^{(e)}|\hat{R}(\mathbf{n}^{(e)}), \tag{19}$$

which is valid for any direction $\mathbf{n}^{(e)}$. Since the summation over spin projections $m^{(e)}$ leads to exclusion of $\mathbf{n}^{(e)}$ in the reduced tomogram (18) (this phenomenon is also known as non-signalling), we draw a conclusion that it is impossible to reconstruct the muonium density matrix by measuring the reduced tomogram (18) only.

However, if we consider the individual unitary two-spin tomogram (15), we will see that the reduced tomogram

$$\widetilde{w}(m^{(\mu)},\hat{U})=\sum_{m^{(e)}=-j^{(e)}}^{j^{(e)}}w(m^{(\mu)},m^{(e)},\hat{U})=\langle j^{(\mu)}m^{(\mu)}|\mathrm{Tr}_e[\hat{U}\ \hat{\rho}\ \hat{U}^{\dagger}]|j^{(\mu)}m^{(\mu)}\rangle \tag{20}$$

does contain the full information about the muonium spin state. The physical meaning of the distribution function (20) is a probability to obtain the muon spin projection on z-axis being equal to $m^{(\mu)}$ after a unitary rotation $\hat{U}$ is fulfilled over the common density operator $\hat{\rho}$. In Sec. 7.1, we will outline how to reconstruct the muonium (and Mu-like) density matrix by using measurable muon tomogram (20), where the role of unitary transformation $\hat{U}$ is played by an evolution operator $\hat{\mathscr{U}}(t)$.

3.2.2 Total Two-Spin Tomogram

From the mathematical point of view, the total unitary two-spin tomogram $w^{(L)}(M,\hat{U})$ is merely a set of diagonal elements of the transformed density operator in the alternative basis of states $|LM\rangle$:

$$w^{(L)}(M,\hat{U})=\langle LM|\hat{U}\ \hat{\rho}\ \hat{U}^{\dagger}|LM\rangle. \tag{21}$$

Nonetheless, the tomogram $w^{(L)}(M,\hat{U})$ has a physical meaning different from that of the individual unitary two-spin tomogram (15). Actually, $w^{(L)}(M,\hat{U})$ is the probability to find the system in L-spin configuration and to obtain the total spin projection onto z-direction equal to M after the density operator $\hat{\rho}$ experiences a unitary transformation $\hat{U}$. Obviously, the tomogram $w^{(L)}(M,\hat{U})$ is normalized, i.e. $\sum_L \sum_{M=-L}^{L} w^{(L)}(M,\hat{U}) = 1$. The total unitary two-spin tomogram (21) contains the same information as the individual unitary two-spin tomogram (15) because both of them are nothing else but diagonal representations of the rotated density operator $\hat{U}\hat{\rho}\hat{U}^{\dagger}$, with the only difference being in the basis used: either $\{|j^{(\mu)}m^{(\mu)}\rangle|j^{(e)}m^{(e)}\rangle\}$ or $\{|LM\rangle\}$.

Similarly to the case of individual two-spin tomography, where we specified the unitary transformation in the factorized form of individual rotations, i.e. $\hat{U}_{\rm ind} = \hat{R}(\mathbf{n}^{(\mu)}) \otimes \hat{R}(\mathbf{n}^{(e)})$, it is tempting to introduce separate rotations of subspaces $\{|L'M'\rangle\}$ and $\{|L''M''\rangle\}$ with $L' \neq L''$. For this reason, we introduce the following operator:

$$\hat{U}_{\rm tot} = \hat{R}^{(L')}(\mathbf{n}_{L'}) \oplus \hat{R}^{(L'')}(\mathbf{n}_{L''}) \oplus \ldots \equiv \bigoplus_{L=|j^{(\mu)}-j^{(e)}|}^{j^{(\mu)}+j^{(e)}} \hat{R}^{(L)}(\mathbf{n}_L), \tag{22}$$

where by sign $\oplus$ we designate the direct sum. This means that the matrix representation $U_{\rm tot}$ of the operator $\hat{U}_{\rm tot}$ in the basis of states $\{|LM\rangle\}$ is block-diagonal, with the L-th block being the $(2L+1) \times (2L+1)$ matrix $R^{(L)}(\mathbf{n}_L)$ defined by formula (4).

It is of vital importance to trace how the problem of addition of angular moments is related with individual and total two-spin tomograms. The result is

$$\bigoplus_{L=|j^{(\mu)}-j^{(e)}|}^{j^{(\mu)}+j^{(e)}} \hat{R}^{(L)}(\mathbf{N}) \equiv \hat{R}^{(L')}(\mathbf{N}) \oplus \hat{R}^{(L'')}(\mathbf{N}) \oplus \ldots = \hat{R}^{(j^{(\mu)})}(\mathbf{N}) \otimes \hat{R}^{(j^{(e)})}(\mathbf{N}) \tag{23}$$

or in the matrix form

$$\bigoplus_{L=|j^{(\mu)}-j^{(e)}|}^{j^{(\mu)}+j^{(e)}} R^{(L)}(\mathbf{N}) \equiv R^{(L')}(\mathbf{N}) \oplus R^{(L'')}(\mathbf{N}) \oplus \ldots = U_{\rm CG}^{\dagger}\ R^{(j^{(\mu)})}(\mathbf{N}) \otimes R^{(j^{(e)})}(\mathbf{N})\ U_{\rm CG}, \tag{24}$$

where $U_{\rm CG}$ is a matrix of Clebsch-Gordon coefficients.

Arguing in the same manner as in case of individual two-spin tomogram (16), we introduce the following total two-spin probability distribution function of the form

$$f^{(L)}(M,\mathbf{N}) = \langle LM| \bigoplus_{L=|j^{(\mu)}-j^{(e)}|}^{j^{(\mu)}+j^{(e)}} \hat{R}^{(L)}(\mathbf{N})\ \hat{\rho} \bigoplus_{L=|j^{(\mu)}-j^{(e)}|}^{j^{(\mu)}+j^{(e)}} \hat{R}^{(L)\dagger}(\mathbf{N})|LM\rangle. \tag{25}$$

It turns out that the knowledge of the probability distribution function (25) is not enough, in general, to reconstruct the system density operator of an arbitrary mixed state [43]. Consequently, we cannot regard the function $f^{(L)}(M,\mathbf{N})$ as a true tomogram. However, if the information in (25) is supplemented by probabilities with which pure states appear in the mixed one, the mapping $\hat{\rho} \longrightarrow f^{(L)}(M,\mathbf{N})$ is proved to be invertible [43].

Despite the probability distribution (25) is not informationally complete, it can still be treated as a tomogram of identical spin-j particles [44]. Indeed, in case of a bipartite system with indistinguishable constituents, the density operator of the whole system ρ is known to be invariant with respect to a particle permutation. Hence, the density matrix in the basis of states $\{|LM\rangle\}$ is block-diagonal and can be reconstructed as follows:

$$\rho_{\ \text{indistinguishable}} \equiv \bigoplus_{L=0}^{2j} \rho^{(L)} = \bigoplus_{L=0}^{2j} \sum_{M=-L}^{L} \int_{S^2} \frac{d\mathbf{N}}{4\pi}\ f^{(L)}(M,\mathbf{N}) \hat{D}^{(L)}(M,\mathbf{N}), \tag{26}$$

where the quantizer $\hat{D}^{(L)}(M,\mathbf{N})$ is determined by formula (7). As far as other aspects of the addition of angular moments in the tomographic-probability representation are beyond the MuSR-method, they will be discussed elsewhere.

In order to conclude this consideration, we derive the relation between the individual two-spin tomogram (16) and the total unitary two-spin tomogram (21)

$$w^{(L)}(M,\hat{U}) = \sum_{m^{(\mu)}=-j^{(\mu)}}^{j^{(\mu)}} \int_{S^2} \frac{d\mathbf{n}^{(\mu)}}{4\pi} \sum_{m^{(e)}=-j^{(e)}}^{j^{(e)}} \int_{S^2} \frac{d\mathbf{n}^{(\mathbf{e})}}{4\pi}\; w(m^{(\mu)},\mathbf{n}^{(\mu)},m^{(e)},\mathbf{n}^{(e)}) \times\langle LM|\hat{U}\;\hat{D}^{(j^{(\mu)})}(m^{(\mu)},\mathbf{n}^{(\mu)})\otimes\hat{D}^{(j^{(e)})}(m^{(e)},\mathbf{n}^{(e)})\;\hat{U}^{\dagger}|LM\rangle. \tag{27}$$

4 Entanglement and Separability in Probability Representation

A state of two-spin system (muon and electron spins) is called separable if the density operator $\hat{\rho}$ of the whole system can be resolved into the following convex sum

$$\hat{\rho}_{\text{separable}} = \sum_i p_i\;\hat{\rho}_i^{(\mu)}\otimes\hat{\rho}_i^{(e)}, \qquad 0\le p_i\le 1, \quad \sum_i p_i = 1, \tag{28}$$

otherwise the state is called entangled. Since the individual two-spin tomogram $w(m^{(\mu)},\mathbf{n}^{(\mu)},m^{(e)},\mathbf{n}^{(e)})$ contains the same information about the system involved, the definition of separability (28) is readily reformulated in terms of tomograms. In fact, the state is separable when

$$w_{\text{separable}}(m^{(\mu)},\mathbf{n}^{(\mu)},m^{(e)},\mathbf{n}^{(e)}) = \sum_i p_i\;w_i^{(j^{(\mu)})}(m^{(\mu)},\mathbf{n}^{(\mu)})w_i^{(j^{(e)})}(m^{(e)},\mathbf{n}^{(e)}). \tag{29}$$

If the resolution (29) is not fulfilled for any convex parameters p_i, then the state is entangled.

4.1 Entanglement Detection via Bell-like Inequality Violation

To detect the entanglement of a two-qubit system it is convenient to check the violation of the following Bell-like inequality (see, e.g. [45]):

$$|B|\le 2, \tag{30}$$

where the Bell-like number B reads

$$B = \text{Tr}\left[\mathscr{I}\begin{pmatrix} w(+,\mathbf{n}_1^{(\mu)},+,\mathbf{n}_1^{(e)}) & w(+,\mathbf{n}_1^{(\mu)},+,\mathbf{n}_2^{(e)}) & w(+,\mathbf{n}_2^{(\mu)},+,\mathbf{n}_1^{(e)}) & w(+,\mathbf{n}_2^{(\mu)},+,\mathbf{n}_2^{(e)}) \\ w(+,\mathbf{n}_1^{(\mu)},-,\mathbf{n}_1^{(e)}) & w(+,\mathbf{n}_1^{(\mu)},-,\mathbf{n}_2^{(e)}) & w(+,\mathbf{n}_2^{(\mu)},-,\mathbf{n}_1^{(e)}) & w(+,\mathbf{n}_2^{(\mu)},-,\mathbf{n}_2^{(e)}) \\ w(-,\mathbf{n}_1^{(\mu)},+,\mathbf{n}_1^{(e)}) & w(-,\mathbf{n}_1^{(\mu)},+,\mathbf{n}_2^{(e)}) & w(-,\mathbf{n}_2^{(\mu)},+,\mathbf{n}_1^{(e)}) & w(-,\mathbf{n}_2^{(\mu)},+,\mathbf{n}_2^{(e)}) \\ w(-,\mathbf{n}_1^{(\mu)},-,\mathbf{n}_1^{(e)}) & w(-,\mathbf{n}_1^{(\mu)},-,\mathbf{n}_2^{(e)}) & w(-,\mathbf{n}_2^{(\mu)},-,\mathbf{n}_1^{(e)}) & w(-,\mathbf{n}_2^{(\mu)},-,\mathbf{n}_2^{(e)}) \end{pmatrix}\right], \tag{31}$$

where the sign $\pm$ denotes spin projection $\pm 1/2$, respectively, and the matrix $\mathscr{I}$ is defined through

$$\mathscr{I} = \begin{pmatrix} 1 & -1 & -1 & 1 \\ 1 & -1 & -1 & 1 \\ 1 & -1 & -1 & 1 \\ -1 & 1 & 1 & -1 \end{pmatrix}. \tag{32}$$

If state is separable, then the inequality (30) is necessarily valid. Thus, its violation is a direct evidence of the system entanglement. Note, that we do not resort to the density matrix formalism while dealing with such an approach.

4.2 Positive Partial Transpose in the Tomographic-Probability Representation

Two-qubit and qubit-qutrit states are known to be separable iff positive partial transpose $\rho^{\rm ppt}$ of the system density matrix ρ results in a new density matrix (Peres-Horodecki criterion [46,47]). If $\rho^{\rm ppt}$ is not a density matrix, this is the direct evidence of the entanglement. The Peres-Horodecki criterion differs substantially from the approach outlined in the previous subsection because it provides the necessary and sufficient condition for a two-qubit state or qubit-qutrit state to be entangled whereas the violation of the Bell-like inequality (30) is only a sufficient but not necessary indicator of entanglement.

Positive partial transpose (PPT) of bipartite state ρ leaves the second subsystem undisturbed and makes a transpose of the first subsystem, which is equivalent to the complex conjugation of the first subsystem (time reversion). Since the complex conjugation of qubit density matrix $\rho = \frac{1}{2}(I + (\mathbf{P}\cdot\boldsymbol{\sigma}))$ boils down to the replacement $P_y \to -P_y$, the corresponding qubit tomogram $w(m,\mathbf{n})$ transforms into $w(m,\mathbf{n}^{\rm ppt})$, where $\mathbf{n}^{\rm ppt} \equiv (n_x, -n_y, n_z)$. Consequently, in case of two qubits (muonium) and qubit-qutrit system (muonium-like system), the action of positive partial transpose on the individual two-spin tomogram (16) is

$$w^{\rm ppt}(m^{(\mu)},\mathbf{n}^{(\mu)},m^{(e)},\mathbf{n}^{(e)}) = w(m^{(\mu)},\mathbf{n}^{(\mu){\rm ppt}},m^{(e)},\mathbf{n}^{(e)}). \tag{33}$$

In the density-matrix formalism, the following step is to check a positivity of the matrix $\rho^{\rm ppt}$. It is shown in [48] that eigenvalues $\{\lambda_i\}_{i=1}^4$ of a 4×4 Hermitian matrix Λ with unit trace (${\rm Tr}\Lambda = 1$) are non-negative iff $M_2 \equiv \sum\limits_{i<j}\lambda_i\lambda_j \geq 0$, $M_3 \equiv \sum\limits_{i<j<k}\lambda_i\lambda_j\lambda_k \geq 0$, and $M_4 \equiv \sum\limits_{i<j<k<l}\lambda_i\lambda_j\lambda_k\lambda_l \geq 0$. Using the trace equality $\sum\limits_i \lambda_i = 1$, these quantities can be expressed through traces ${\rm Tr}\Lambda^n$ as follows:

$$M_2 = \frac{1}{2}\left(1 - {\rm Tr}\Lambda^2\right) \geq 0, \tag{34}$$

$$M_3 = \frac{1}{6}\left(1 - 3{\rm Tr}\Lambda^2 + 2{\rm Tr}\Lambda^3\right) \geq 0, \tag{35}$$

$$M_4 = \frac{1}{24}\left(1 - 6{\rm Tr}\Lambda^2 + 3\left[{\rm Tr}\Lambda^2\right]^2 + 8{\rm Tr}\Lambda^3 - 6{\rm Tr}\Lambda^4\right) \geq 0. \tag{36}$$

Substituting $\rho^{\rm ppt}$ for Λ in (34)–(36), it is possible to detect unambiguously the entanglement of two-qubit system by observing a violation of at least one inequality. The value of M_2 turns out to be invariant with respect to PPT transformation. In view of this, we introduce the following entanglement measure E for two qubits:

$$E = |M_3| + |M_4| - M_3 - M_4. \tag{37}$$

In the tomographic-probability approach, the values of M_3 and M_4 read

$$M_3 = \frac{1}{6}\sum_{m^{(\mu)}}\sum_{m^{(e)}}[w^{\rm ppt} - 3w^{\rm ppt}\star w^{\rm ppt} + 2w^{\rm ppt}\star w^{\rm ppt}\star w^{\rm ppt}](m^{(\mu)},\mathbf{n}^{(\mu)},m^{(e)},\mathbf{n}^{(e)}), \tag{38}$$

$$M_4 = \frac{1}{24}\Bigg(3\Big(\sum_{m^{(\mu)}}\sum_{m^{(e)}}[w^{\rm ppt}\star w^{\rm ppt}](m^{(\mu)},\mathbf{n}^{(\mu)},m^{(e)},\mathbf{n}^{(e)})\Big)^2 + \sum_{m^{(\mu)}}\sum_{m^{(e)}}[w^{\rm ppt} - 6w^{\rm ppt}\star w^{\rm ppt}$$
$$+8w^{\rm ppt}\star w^{\rm ppt}\star w^{\rm ppt} - 6w^{\rm ppt}\star w^{\rm ppt}\star w^{\rm ppt}\star w^{\rm ppt}](m^{(\mu)},\mathbf{n}^{(\mu)},m^{(e)},\mathbf{n}^{(e)})\Bigg), \tag{39}$$

where by $\star$ we denote a star product with the kernel

$$K(m_1'\mathbf{n}_1'm_2'\mathbf{n}_2', m_1''\mathbf{n}_1''m_2''\mathbf{n}_2'', m_1\mathbf{n}_1m_2\mathbf{n}_2) = \prod_{i=1}^{2}\Big[\frac{1}{4} + 9m_i'm_i''\left(\mathbf{n}_i'\cdot\mathbf{n}_i''\right) + 3m_im_i'\left(\mathbf{n}_i\cdot\mathbf{n}_i'\right)$$
$$+3m_im_i''\left(\mathbf{n}_i\cdot\mathbf{n}_i''\right) + i18m_im_i'm_i''\left(\mathbf{n}_i\cdot[\mathbf{n}_i'\times\mathbf{n}_i'']\right)\Big]. \tag{40}$$

Thus, the measure (37) is expressed through spin tomograms only.

5 Evolution of Tomograms

Evolution of pure states $|\psi\rangle$ is governed by Schrödinger equation $i\hbar\frac{\partial|\psi\rangle}{\partial t} = \hat{H}|\psi\rangle$, where $\hat{H}$ is a Hamiltonian of the system. If we consider generally mixed state with the density operator $\hat{\rho}$, the evolution obeys the von Neumann equation $i\hbar\frac{\partial\hat{\rho}}{\partial t} = [\hat{H}, \hat{\rho}]$ which is similar to Liuville equation in classical statistical mechanics. Taking advantage of mapping $\hat{\rho}(t) \longrightarrow w(m, \hat{u}, t)$ for a single spin-j particle (Eq. (3)), the von Neumann equation with the initial condition takes the form

$$i\hbar\frac{\partial w(m,\hat{u},t)}{\partial t} = [f_H \star w - w \star f_H](m,\hat{u},t), \qquad w(m,\hat{u},t=0) = w_0(m,\hat{u}), \tag{41}$$

where $f_H(m, \hat{u}, t)$ is a tomographic symbol of operator $\hat{H}$ obtained by replacing $\hat{\rho} \to \hat{H}$ in formula (3); a star $\star$ implies the so-called star product of tomographic symbols. In other words,

$$[f_H \star w](m,\hat{u},t) = \sum_{m',m''=-j}^{j} \int d\hat{u}' \int d\hat{u}'' f_H(m',\hat{u}',t) f_H(m',\hat{u}',t) K(m',\hat{u}',m'',\hat{u}'',m,\hat{u}), \tag{42}$$

where $\int d\hat{u}$ is an integration over the corresponding measure, $K(m', \hat{u}', m'', \hat{u}'', m, \hat{u})$ is the star-product kernel of the form $K = Tr\big[\hat{D}(m',\hat{u}')\hat{D}(m'',\hat{u}'')\hat{U}(m,\hat{u})\big]$, where $\hat{D}$ and $\hat{U}$ are quantizer and dequantizer operators, respectively. Explicit form of the spin tomographic star-product kernel is found in [25, 26, 34].

Formal solutions of Schrödinger and von Neumann equations are expressed through the unitary evolution operator $\hat{\mathscr{U}}(t)$ as follows:

$$|\psi(t)\rangle = \hat{\mathscr{U}}(t)|\psi(0)\rangle, \qquad \hat{\rho}(t) = \hat{\mathscr{U}}(t)\hat{\rho}(0)\hat{\mathscr{U}}^{\dagger}(t), \tag{43}$$

$$\hat{\mathscr{U}}(t) = \hat{T}\exp\left[-\frac{i}{\hbar}\int_0^t \hat{H}(\tau)d\tau\right], \tag{44}$$

where $\hat{T}$ is a time-ordering operator.

Using the relation (43) as well as the mapping (3), it is not hard to see that the time evolution of a unitary spin tomogram reads

$$w(m,\hat{u},t) = w_0(m,\hat{u}\hat{\mathscr{U}}(t)). \tag{45}$$

which is nothing else but the formal solution of the tomographic evolution equation (41).

As far as muonium and muonium-like systems are concerned, the evolution of the individual unitary two-spin tomogram (15) reads

$$w(m^{(\mu)}, m^{(e)}, \hat{U}, t) = w_0(m^{(\mu)}, m^{(e)}, \hat{U}\hat{\mathscr{U}}(t)), \tag{46}$$

whereas the evolution of the individual two-spin tomogram (16) has a rather complicated form

$$\begin{aligned} &w(m^{(\mu)}, \mathbf{n}^{(\mu)}, m^{(e)}, \mathbf{n}^{(e)}, t) \\ &= \sum_{\widetilde{m}^{(\mu)}=-j^{(\mu)}}^{j^{(\mu)}} \int_{S^2} \frac{d\widetilde{\mathbf{n}}^{(\mu)}}{4\pi} \sum_{\widetilde{m}^{(e)}=-j^{(e)}}^{j^{(e)}} \int_{S^2} \frac{d\widetilde{\mathbf{n}}^{(e)}}{4\pi}\; w_0(\widetilde{m}^{(\mu)}, \widetilde{\mathbf{n}}^{(\mu)}, \widetilde{m}^{(e)}, \widetilde{\mathbf{n}}^{(e)})\; \langle j^{(\mu)}m^{(\mu)}, j^{(e)}m^{(e)}|\hat{R}(\mathbf{n}^{(\mu)}) \otimes \hat{R}(\mathbf{n}^{(e)}) \\ &\times \hat{\mathscr{U}}(t)\hat{D}^{(j^{(\mu)})}(\widetilde{m}^{(\mu)}, \widetilde{\mathbf{n}}^{(\mu)}) \otimes \hat{D}^{(j^{(e)})}(\widetilde{m}^{(e)}, \widetilde{\mathbf{n}}^{(e)})\hat{\mathscr{U}}^{\dagger}(t)\; \hat{R}^{\dagger}(\mathbf{n}^{(\mu)}) \otimes \hat{R}^{\dagger}(\mathbf{n}^{(e)})|j^{(\mu)}m^{(\mu)}, j^{(e)}m^{(e)}\rangle. \end{aligned} \tag{47}$$

6 Muonium and Mu-like Systems: Hamiltonian

Hamiltonian of a muonium-like system has the following most general form:

$$\hat{H}_{\text{general}}(q,s) = \hat{H}_0(q) + \hat{V}(q,s), \tag{48}$$

where q and s are responsible for position and spin variables, respectively; $\hat{H}_0(q)$ is a part depending on space coordinates only; and $\hat{V}(q,s)$ is a part containing spin variables. For muonium-like systems, Coulomb and spin-orbital interactions are much greater than the hyperfine interaction ($H_0 \gg V$). For this reason, in our case the operator $\hat{V}(q,s)$ will only contain the hyperfine interaction and an interaction of magnetic moments μ_μ and μ_e with local magnetic fields. On averaging over space coordinates, the operator $\langle\psi(q)|\hat{V}(q,s)|\psi(q)\rangle$ acts on spin degrees of freedom, i.e., it can be represented by $N \times N$ spin-Hamiltonian operator $\hat{H}$ with $N = (2j^{(\mu)}+1)(2j^{(e)}+1)$.

6.1 Muonium Hamiltonian

We will consider three main kinds of muonium Hamiltonian:

- Free muonium atom in vacuum is governed by hyperfine interaction

$$\hat{H}_{\rm hf} = \hbar\omega_0(\hat{\mathbf{J}}^{(\mu)} \odot \hat{\mathbf{J}}^{(e)}) \equiv \hbar\omega_0(\hat{J}_x^{(\mu)} \otimes \hat{J}_x^{(e)} + \hat{J}_y^{(\mu)} \otimes \hat{J}_y^{(e)} + \hat{J}_z^{(\mu)} \otimes \hat{J}_z^{(e)}), \tag{49}$$

  where the frequency of hyperfine interaction $\omega_0 = 4453$ MHz. It is worth mentioning that such a Hamiltonian provides an adequate description of muonium not only in vacuum but also in quartz and ice. Frequency of hyperfine splitting in such materials is almost the same as in vacuum within the accuracy of the experiment. The correction caused by interaction of the electron quadrupole electrical moment with inhomogeneous crystal field can lead to anisotropic Hamiltonian (in quartz at temperatures $T \lesssim 100$ K).

- Isotropic Hamiltonian of a muonium-like system in solids in presence of magnetic field $\mathbf{B}$

$$\hat{H}_{\rm Mu} = A(\hat{\mathbf{J}}^{(\mu)} \odot \hat{\mathbf{J}}^{(e)}) - g_\mu\mu_\mu(\mathbf{B}\cdot\hat{\mathbf{J}}^{(\mu)}) \otimes \hat{I}^{(e)} + g_e\mu_e\hat{I}^{(\mu)} \otimes (\mathbf{B}\cdot\hat{\mathbf{J}}^{(e)}), \tag{50}$$

  where in general $A \neq \hbar\omega_0$, $g_\mu = 2$, μ_e is the Bohr magneton, and $(\mathbf{B}\cdot\hat{\mathbf{J}}) \equiv B_x\hat{J}_x + B_y\hat{J}_y + B_z\hat{J}_z$.

- Anisotropic Hamiltonian of anomalous muonium (Mu*) which is present, for instance, in Si and many other semiconductors with a diamond structure of crystal lattice

$$\hat{H}_{\rm Mu^*} = \hat{H}_{\rm Mu} + \Delta A(\mathfrak{N}\cdot\hat{\mathbf{J}}^{(\mu)}) \otimes (\mathfrak{N}\cdot\hat{\mathbf{J}}^{(e)}), \tag{51}$$

  where $\mathfrak{N}$ is a unit vector determining the axis of axial asymmetry.

If the Hamiltonian is time-independent (magnetic field is steady), then the corresponding unitary evolution operators can be found analytically. In the basis of states $|j^{(\mu)}m^{(\mu)}, j^{(e)}m^{(e)}\rangle$, the unitary evolution matrix of hyperfine interaction reads

$$\mathscr{U}_{\rm hf}(t) = \frac{1}{2}e^{-i\omega_0 t/4}\begin{pmatrix} 2 & 0 & 0 & 0 \\ 0 & 1+e^{i\omega_0 t} & 1-e^{i\omega_0 t} & 0 \\ 0 & 1-e^{i\omega_0 t} & 1+e^{i\omega_0 t} & 0 \\ 0 & 0 & 0 & 2 \end{pmatrix} \tag{52}$$

In order to find the evolution matrix of Mu in presence of magnetic field, the intensity $\mathbf{B}$ is chosen to be aligned along z-direction, i.e. $\mathbf{B} \parallel z$ (longitudinal field). In this case, we obtain

$$\mathscr{U}_{{\rm Mu}\ z}(t) = e^{iat}\begin{pmatrix} e^{-i(2a-b_-)t} & 0 & 0 & 0 \\ 0 & \cos ct + i(b_+/c)\sin ct & -i(2a/c)\sin ct & 0 \\ 0 & -i(2a/c)\sin ct & \cos ct - i(b_+/c)\sin ct & 0 \\ 0 & 0 & 0 & e^{-i(2a+b_-)t} \end{pmatrix}, \tag{53}$$

where $a = A/(4\hbar)$, $b_\pm = B(g_\mu\mu_\mu \pm g_e\mu_e)/(2\hbar)$, and $c = \sqrt{A^2 + B^2(g_\mu\mu_\mu + g_e\mu_e)^2}/(2\hbar)$.

If the magnetic field is aligned along x-axis (transversal field), the unitary evolution matrix $\mathscr{U}_{\mathrm{Mu}\ x}(t)$ is symmetrical, and its matrix elements read

$$[\mathscr{U}_{\mathrm{Mu}\ x}(t)]_{11} = [\mathscr{U}_{\mathrm{Mu}\ x}(t)]_{44} = \frac{1}{2}\left[e^{-iat}\cos b_- t + e^{iat}\left(\cos ct - i(2a/c)\sin ct\right)\right], \tag{54}$$

$$[\mathscr{U}_{\mathrm{Mu}\ x}(t)]_{22} = [\mathscr{U}_{\mathrm{Mu}\ x}(t)]_{33} = \frac{1}{2}\left[e^{-iat}\cos b_- t + e^{iat}\left(\cos ct + i(2a/c)\sin ct\right)\right], \tag{55}$$

$$[\mathscr{U}_{\mathrm{Mu}\ x}(t)]_{12} = [\mathscr{U}_{\mathrm{Mu}\ x}(t)]_{34} = -\frac{i}{2}\left[e^{-iat}\sin b_- t + (b_+/c)e^{iat}\sin ct\right], \tag{56}$$

$$[\mathscr{U}_{\mathrm{Mu}\ x}(t)]_{13} = [\mathscr{U}_{\mathrm{Mu}\ x}(t)]_{24} = -\frac{i}{2}\left[e^{-iat}\sin b_- t - (b_+/c)e^{iat}\sin ct\right], \tag{57}$$

$$[\mathscr{U}_{\mathrm{Mu}\ x}(t)]_{14} = \frac{1}{2}\left[e^{-iat}\cos b_- t - e^{iat}\left(\cos ct - i(2a/c)\sin ct\right)\right], \tag{58}$$

$$[\mathscr{U}_{\mathrm{Mu}\ x}(t)]_{23} = \frac{1}{2}\left[e^{-iat}\cos b_- t - e^{iat}\left(\cos ct + i(2a/c)\sin ct\right)\right]. \tag{59}$$

Finally, if direction of the magnetic field coincides with y-axis, the unitary evolution matrix $\mathscr{U}_{\mathrm{Mu}\ y}(t)$ is expressed through matrix $\mathscr{U}_{\mathrm{Mu}\ x}(t)$ as follows:

$$\mathscr{U}_{\mathrm{Mu}\ y}(t) = \begin{pmatrix} [\mathscr{U}_{\mathrm{Mu}\ x}(t)]_{11} & -i[\mathscr{U}_{\mathrm{Mu}\ x}(t)]_{12} & -i[\mathscr{U}_{\mathrm{Mu}\ x}(t)]_{13} & -[\mathscr{U}_{\mathrm{Mu}\ x}(t)]_{14} \\ i[\mathscr{U}_{\mathrm{Mu}\ x}(t)]_{21} & [\mathscr{U}_{\mathrm{Mu}\ x}(t)]_{22} & [\mathscr{U}_{\mathrm{Mu}\ x}(t)]_{23} & -i[\mathscr{U}_{\mathrm{Mu}\ x}(t)]_{24} \\ i[\mathscr{U}_{\mathrm{Mu}\ x}(t)]_{31} & [\mathscr{U}_{\mathrm{Mu}\ x}(t)]_{32} & [\mathscr{U}_{\mathrm{Mu}\ x}(t)]_{33} & -i[\mathscr{U}_{\mathrm{Mu}\ x}(t)]_{34} \\ -[\mathscr{U}_{\mathrm{Mu}\ x}(t)]_{41} & i[\mathscr{U}_{\mathrm{Mu}\ x}(t)]_{42} & i[\mathscr{U}_{\mathrm{Mu}\ x}(t)]_{43} & [\mathscr{U}_{\mathrm{Mu}\ x}(t)]_{44} \end{pmatrix}. \tag{60}$$

As concerns the anisotropic hyperfine interaction (51), we will present below the explicit analytical solutions for three cases. The first one is $\mathfrak{N} \parallel z$ and $\mathbf{B} \parallel z$, in this case we obtain the following unitary evolution matrix $\mathscr{U}_{\mathrm{Mu}^* zz}(t)$:

$$\mathscr{U}_{\mathrm{Mu}^* zz}(t) = e^{i(a+d)t}\begin{pmatrix} e^{-i(2(a+d)-b_-)t} & 0 & 0 & 0 \\ 0 & \cos ct + i(b_+/c)\sin ct & -i(2a/c)\sin ct & 0 \\ 0 & -i(2a/c)\sin ct & \cos ct - i(b_+/c)\sin ct & 0 \\ 0 & 0 & 0 & e^{-i(2(a+d)+b_-)t} \end{pmatrix}, \tag{61}$$

where $d = \Delta A/(4\hbar)$.

In case $\mathfrak{N} \parallel x$ and $\mathbf{B} \parallel z$, we obtain symmetrical matrix $\mathscr{U}_{\mathrm{Mu}^* xz}(t)$ with the elements

$$[\mathscr{U}_{\mathrm{Mu}^* xz}(t)]_{11} = e^{-iat}\big[\cos ft + i(b_-/f)\sin ft\big], \tag{62}$$

$$[\mathscr{U}_{\mathrm{Mu}^* xz}(t)]_{12} = [\mathscr{U}_{\mathrm{Mu}^* xz}(t)]_{13} = [\mathscr{U}_{\mathrm{Mu}^* xz}(t)]_{24} = [\mathscr{U}_{\mathrm{Mu}^* xz}(t)]_{34} = 0, \tag{63}$$

$$[\mathscr{U}_{\mathrm{Mu}^* xz}(t)]_{14} = -ie^{-iat}(d/f)\sin ft, \tag{64}$$

$$[\mathscr{U}_{\mathrm{Mu}^* xz}(t)]_{22} = e^{iat}\big[\cos ht + i(b_+/h)\sin ht\big], \tag{65}$$

$$[\mathscr{U}_{\mathrm{Mu}^* xz}(t)]_{23} = -ie^{iat}[(2a+d)/h]\sin ht, \tag{66}$$

$$[\mathscr{U}_{\mathrm{Mu}^* xz}(t)]_{33} = e^{iat}\big[\cos ht - i(b_+/h)\sin ht\big], \tag{67}$$

$$[\mathscr{U}_{\mathrm{Mu}^* xz}(t)]_{44} = e^{-iat}\big[\cos ft + i(b_-/f)\sin ft\big], \tag{68}$$

where $f = \sqrt{(\Delta A)^2 + 4B^2(g_\mu\mu_\mu - g_e\mu_e)^2}/(4\hbar)$ and $h = \sqrt{(A + \Delta A/2)^2 + B^2(g_\mu\mu_\mu + g_e\mu_e)^2}/(2\hbar)$.

Finally, in case $\mathfrak{N} \parallel y$ and $\mathbf{B} \parallel z$, we obtain the symmetrical unitary evolution matrix $\mathscr{U}_{\mathrm{Mu}^* yz}(t)$ whose elements coincide with elements of the matrix $\mathscr{U}_{\mathrm{Mu}^* xz}(t)$ except for $[\mathscr{U}_{\mathrm{Mu}^* yz}(t)]_{14} = -[\mathscr{U}_{\mathrm{Mu}^* xz}(t)]_{14}$.

6.2 Mu-like Hamiltonian

The muonium-like systems are described by Hamiltonians (49)–(51), where the effective moment of the electron shell $j^{(e)}$ is greater than 1/2, i.e. the dimension of the operator $\hat{\mathbf{J}}^{(e)}$ is greater than 2. In the particular case $j^{(e)} = 1$, the effective hyperfine interaction will result in the following unitary evolution matrix:

$$\mathscr{U}_{\text{hf }\mu-\text{like}}(t) = \begin{pmatrix} \mathscr{V}_1 & 0 & 0 & 0 & 0 & 0 \\ 0 & \mathscr{V}_- & 0 & \mathscr{V}_2 & 0 & 0 \\ 0 & 0 & \mathscr{V}_+ & 0 & \mathscr{V}_2 & 0 \\ 0 & \mathscr{V}_2 & 0 & \mathscr{V}_+ & 0 & 0 \\ 0 & 0 & \mathscr{V}_2 & 0 & \mathscr{V}_- & 0 \\ 0 & 0 & 0 & 0 & 0 & \mathscr{V}_1 \end{pmatrix}, \tag{69}$$

where matrix elements $\mathscr{V}$ are expressed through the strength of hyperfine interaction A

$$\mathscr{V}_1 = e^{-iAt/(2\hbar)}, \qquad \mathscr{V}_2 = -ie^{iAt/(4\hbar)}(2\sqrt{2}/3)\sin(3At/(4\hbar)), \tag{70}$$

$$\mathscr{V}_\pm = e^{iAt/(4\hbar)}\big[\cos(3At/(4\hbar)) \pm (i/3)\sin(3At/(4\hbar))\big]. \tag{71}$$

The entanglement of a Mu-like systems can be detected by using tomogram $w(m^{(\mu)}, \mathbf{n}^{(\mu)}, m^{(e)}, \mathbf{n}^{(e)})$ together with the qubit portrait method [45] and Bell-like inequality (30). Moreover, PPT inequalities (34)–(36) are necessary conditions for separability, so the non-zero value of quantity (37) is a direct indicator of the entanglement of a Mu-like system as well.

It is worth noting, that we restrict ourselves to the unitary evolution of muonium-like systems and do not consider relaxation processes. Their influence on system behavior and entanglement will be discussed elsewhere.

7 Evolution and Entanglement of Mu-like Systems

In this section, we exploit the developed tomographic approach to solve the problem of evolution and entanglement of Mu, Mu*, and Mu-like systems. We are going to indicate entanglement of Mu-like systems and propose experimentally accessible techniques for creation of entangled states. These two points can be used in order to check experimentally Bell inequalities with solid state spin states.

Let us consider the muonium atom.

As it is shown in Sec. 5, for a given Hamiltonian, the evolution is thoroughly determined by the initial state of a system. In order to demonstrate how the developed method works, we focus on the simplest and physically clear initial state. Since the retarding time of muons in solids is $\sim 10^{-10}$ s, the muons conserve their polarization and are assumed 100% polarized. In contrast, during the formation of muonium the captured electrons have either up or down spin-z projection, i.e. the electron subsystem is in the maximally mixed state (non-coherent mixture). The reference time $t = 0$ is the formation of a muonium. The initial state of a muonium is

$$\hat{\rho}(0) = |\Uparrow\rangle\langle\Uparrow| \otimes \frac{1}{2}\hat{I}^{(e)}. \tag{72}$$

Consequently, the initial individual two-spin tomogram (16) reads

$$w_0(m^{(\mu)}, \mathbf{n}^{(\mu)}, m^{(e)}, \mathbf{n}^{(e)}) = \frac{1}{2}\left(\frac{1}{2} + m^{(\mu)} n_z^{(\mu)}\right), \tag{73}$$

that is the state is factorized (simply separable) and tomogram (73) does not depend on the variables $m^{(e)}$ and $\mathbf{n}^{(e)}$ ascribed to the electron. Substituting the initial tomogram (73) for $w_0(\widetilde{m}^{(\mu)}, \widetilde{\mathbf{n}}^{(\mu)}, \widetilde{m}^{(e)}, \widetilde{\mathbf{n}}^{(e)})$ in

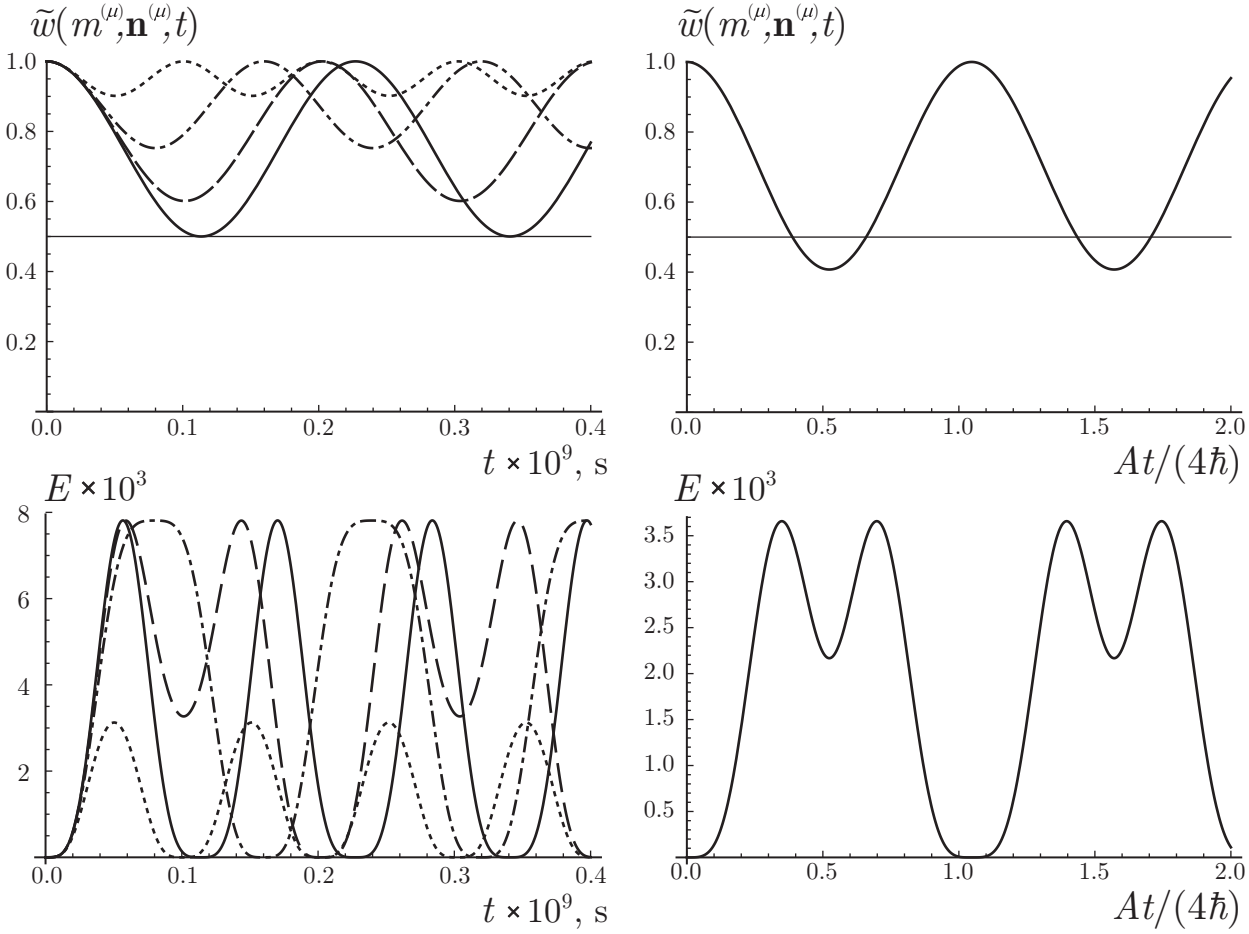

Figure 2: Time evolution of the reduced tomogram $\widetilde{w}(1/2,\mathbf{n}^{(\mu)},t)$ of Mu in quartz (left-up) and Mu-like system with effective electron moment $j^{(e)}=1$ (right-up). Curved lines correspond to $\mathbf{n}^{(\mu)}\parallel z$, horizontal (fine solid) lines correspond to $\mathbf{n}^{(\mu)}\parallel x$ and $\mathbf{n}^{(\mu)}\parallel y$. Time dependence of entanglement for Mu in quartz (left-bottom) and for Mu-like system (right-bottom). The initial state is chosen to be $(2j^{(e)}+1)^{-1}|\Uparrow\rangle\langle\Uparrow|\otimes\hat{I}^{(e)}$. Longitudinal magnetic field $\mathbf{B}\parallel z$ with magnitude $B=0$ (heavy solid line), $B=790$ Gs (dashed line), $B=1580$ Gs (chain line), and $B=3160$ Gs (dotted line).

(47) and separating variables $\{\widetilde{m}^{(\mu)},\widetilde{\mathbf{n}}^{(\mu)}\}$ and $\{\widetilde{m}^{(e)},\widetilde{\mathbf{n}}^{(e)}\}$, we readily obtain a solution in the form of the time-dependent tomogram

$$w(m^{(\mu)},\mathbf{n}^{(\mu)},m^{(e)},\mathbf{n}^{(e)},t) = \frac{1}{4}\Big[1+\langle j^{(\mu)}m^{(\mu)},j^{(e)}m^{(e)}|\hat{R}(\mathbf{n}^{(\mu)})\otimes\hat{R}(\mathbf{n}^{(e)}) \times\hat{\mathscr{U}}(t)\hat{\sigma}_z^{(\mu)}\otimes\hat{I}^{(e)}\hat{\mathscr{U}}^{\dagger}(t)\ \hat{R}^{\dagger}(\mathbf{n}^{(\mu)})\otimes\hat{R}^{\dagger}(\mathbf{n}^{(e)})|j^{(\mu)}m^{(\mu)},j^{(e)}m^{(e)}\rangle\Big], \quad (74)$$

which is suitable to describe the evolution of muonium governed by any unitary evolution (52)– (62).

Let us first consider the evolution in approximation of hyperfine interaction with Hamiltonian (49).

On substituting the unitary evolution matrix (52) for $\mathscr{U}(t)$ in (74), the direct calculation yields

$$w(m^{(\mu)},\mathbf{n}^{(\mu)},m^{(e)},\mathbf{n}^{(e)},t) = \frac{1}{4}\Big(1+m^{(\mu)}n_z^{(\mu)}+m^{(e)}n_z^{(e)}+(m^{(\mu)}n_z^{(\mu)}-m^{(e)}n_z^{(e)})\cos\omega_0 t +2m^{(\mu)}m^{(e)}[\mathbf{n}^{(\mu)}\times\mathbf{n}^{(e)}]_z\sin\omega_0 t\Big). \quad (75)$$

As mentioned in Sec. 3.2.1, the MuSR-experiment enables us to measure the reduced tomogram (tomogram of muon subsystem). In case of the hyperfine interaction evolution, the reduced tomogram reads

$$\widetilde{w}(m^{(\mu)},\mathbf{n}^{(\mu)},t)=\frac{1}{2}\left[1+m^{(\mu)}n_z^{(\mu)}(1+\cos\omega_0 t)\right]. \tag{76}$$

The last term in formula (75) is responsible for entanglement of muon and electron spins. The direct calculation shows that the maximum Bell-like number (30) for tomogram (75) is $\max_{\mathbf{n}_{1,2}^{(\mu,e)}} B=|\sin\omega_0 t|$. Thus, the Bell number satisfies $|B|\leq 1$ and is unappropriate for detecting entanglement of free muonium. Partly, it is due to the initial state (72)–(73) which is obviously mixed whereas the operation of the Bell-like number is best in case of pure states. Applying the PPT criterion to the tomogram (75), we obtain $E=(1/128)\sin^4\omega_0 t$, which reveals the entanglement of a free muonium at the time moments $t\neq \pi k/\omega_0$, $k=0,1,2,\ldots$ Time evolution of the reduced tomogram and the entanglement measure is visualized in Fig. 2 (muonium in quartz, zero field).

Dealing with more complicated systems, for the sake of brevity, we will omit analytical solutions of the tomographic evolution equation (47) and calculations of the entanglement measure (37).

In Fig. 2, we present the reduced (muon) tomogram and the entanglement measure for the simplest Mu-like system "muon + spin 1" which is governed by unitary evolution (69).

As far as muonium in quartz is concerned, we exploit the Hamiltonian (50) with $A=(2\pi\hbar)\cdot 4404$ MHz and different magnetic fields $B=0, B_c/2, B_c, 2B_c$, where $B_c=1580$ Gs is a critical field, i.e. $B(g_e\mu_e-g_\mu\mu_\mu)=A$. In Fig. 2, we illustrate the behavior of the observed reduced tomogram $\widetilde{w}(m^{(\mu)},\mathbf{n}^{(\mu)},t)$ and the entanglement measure E when $\mathbf{B}\parallel z$ (longitudinal field). While increasing the magnetic field intensity B, the tomographic value $\widetilde{w}(m^{(\mu)}=1/2,\mathbf{n}_z^{(\mu)},t)$ oscillates with increasing frequency and tends to 1 due to a preferable muon spin polarization along positive z-axis and electron spin polarization along negative z-axis (separable state). For the same reason, the entanglement measure E decreases substantially when the strength of magnetic filed is greater than the critical value B_c. The probability to obtain muon spin projection $+1/2$ along x- or y-axis is exactly $1/2$ and is not sensitive to the magnitude of magnetic field aligned along z-axis.

The case of muonium in quartz, $\mathbf{B}\parallel x$ (transversal field) is depicted in Fig. 3. Both tomographic values $\widetilde{w}(1/2,\mathbf{n}_z^{(\mu)},t)$ and $\widetilde{w}(1/2,\mathbf{n}_x^{(\mu)},t)$ exhibit a rather complicated dynamics, whereas $\widetilde{w}(1/2,\mathbf{n}_y^{(\mu)},t)=1/2$. Again, the essential decrease of entanglement is observed when $B>B_c$.

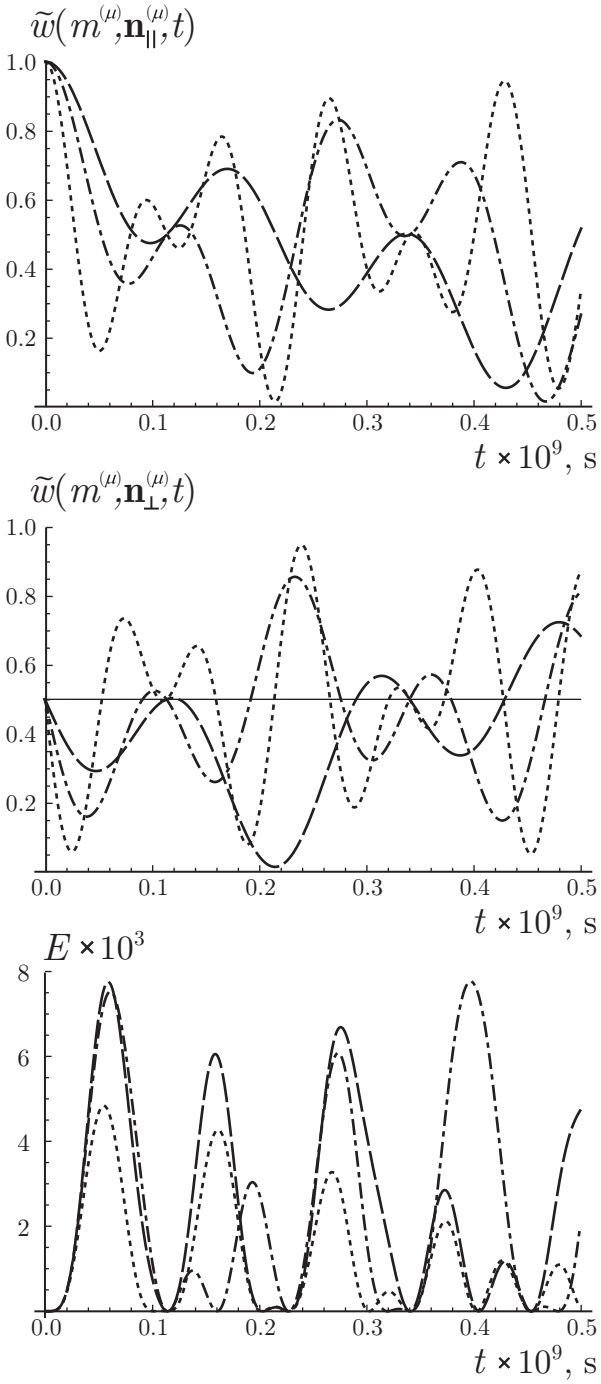

Figure 3: Time evolution of the reduced tomogram $\widetilde{w}(1/2,\mathbf{n}^{(\mu)},t)$ of Mu in quartz with $\mathbf{n}^{(\mu)}\parallel z$ (up), $\mathbf{n}^{(\mu)}\parallel x$ (middle, curved lines), and $\mathbf{n}^{(\mu)}\parallel y$ (middle, horizontal fine solid line). Time dependence of entanglement for Mu in quartz (bottom). The initial state is $|\Uparrow\rangle\langle\Uparrow|\otimes\frac{1}{2}\hat{I}^{(e)}$. Transversal magnetic field $\mathbf{B}\parallel x$ with magnitude $B=790$ Gs (dashed line), $B=1580$ Gs (chain line), and $B=3160$ Gs (dotted line).

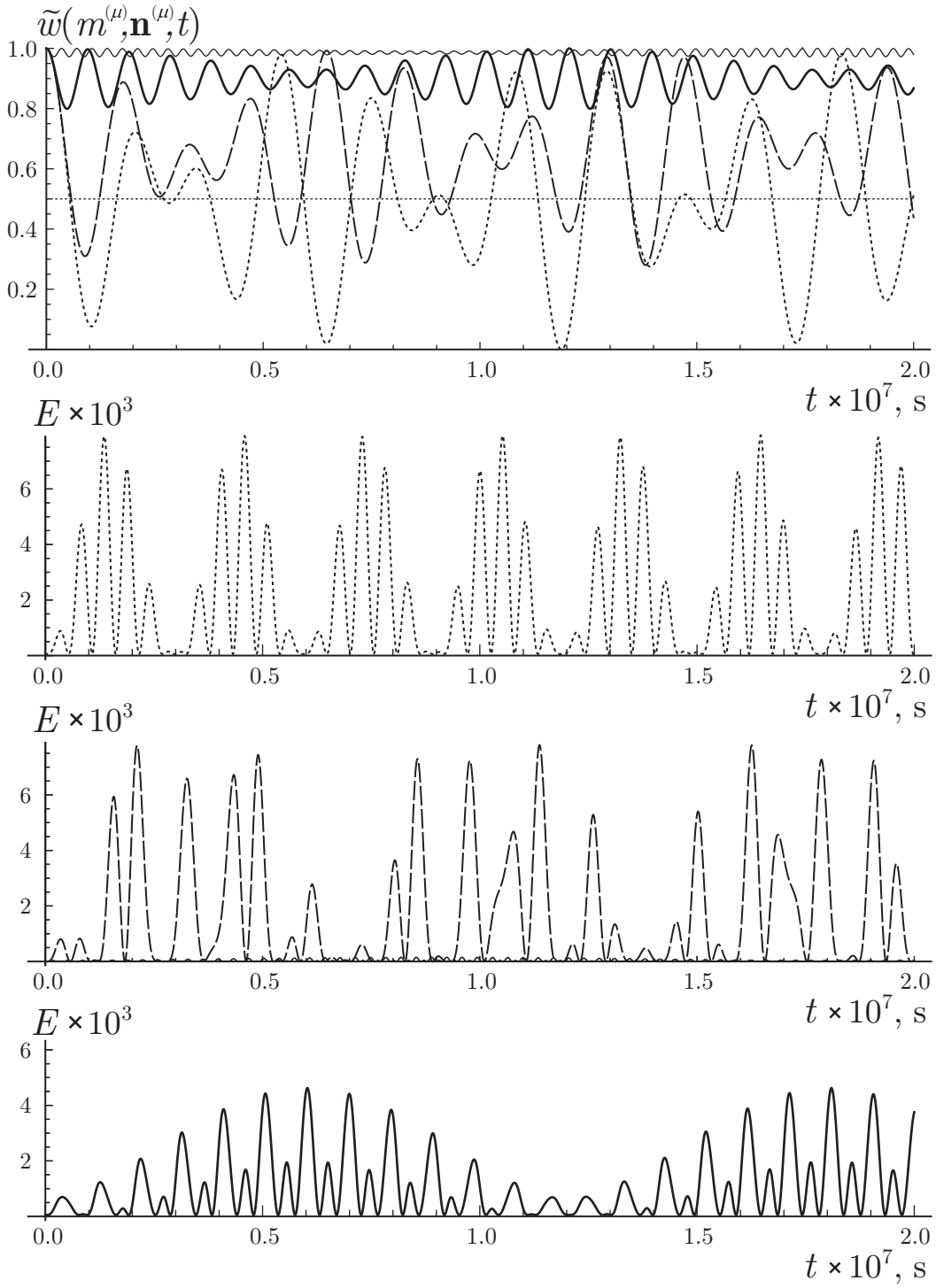

Figure 4: Time evolution of the reduced tomogram $\widetilde{w}(1/2, \mathbf{n}^{(\mu)}, t)$ of Mu* in Si with $\mathbf{n}^{(\mu)} \parallel z$ (up, curved lines), $\mathbf{n}^{(\mu)} \parallel x$ and $\mathbf{n}^{(\mu)} \parallel y$ (up, horizontal fine dotted line). Time dependence of entanglement for Mu* in Si (three bottom figures). The initial state is $|\Uparrow\rangle\langle\Uparrow| \otimes \frac{1}{2}\hat{I}^{(e)}$. Anisotropy direction $\mathfrak{N} \parallel x$. Longitudinal magnetic field $\mathbf{B} \parallel z$ with magnitude $B = 0$ (dotted line), $B = 10$ Gs (dashed line), $B = 33$ Gs (heavy solid line), and $B = 100$ Gs (fine solid line).

Anomalous muonium behaves as an ordinary muonium if $\mathfrak{M} \parallel z$ and $\mathbf{B} \parallel z$, with the only difference being in time scale. The case $\mathfrak{M} \parallel x$ and $\mathbf{B} \parallel z$ is illustrated in Fig. 4, we depict the reduced tomogram and entanglement evolution for anomalous muonium in silicon ($A = 92.595$ MHz, $\Delta A = -75.776$ MHz [49,50]) in presence of different magnetic fields $B = 0$, 10, 33, and 100 Gs (critical field $B_c = 33$ Gs). A two-frequency modulation of the reduced tomogram and a decrease of entanglement are observed if $B \geq B_c$.

7.1 Reconstruction of the Initial State

The strong dependence of the reduced (muon) spin tomogram on time can serve as an indicator of a system Hamiltonian and allows to determine numerical values of parameters (A, ΔA, $\mathbf{B}$, $\mathfrak{M}$). Given the evolution operator $\hat{\mathscr{U}}(t)$ and the measured reduced tomogram $\widetilde{w}(m^{(\mu)}, \mathbf{n}^{(\mu)}, t)$, it is possible, in general, to reconstruct the initial state $\hat{\rho}(0)$ [51]. Indeed, fifteen independent values $\{\widetilde{w}(1/2, \mathbf{n}_k^{(\mu)}, t_l)\}$, $k = x, y, z$, $l = 1, 2, \ldots, 5$ allow the reconstruction of fifteen independent real parameters of 4×4 density matrix $\rho(0)$. The requirement on time moments $\{t_l\}_{l=1}^5$ is to avoid a periodical coincidence. The important requirement on unitary evolution $\hat{\mathscr{U}}(t)$ is to break an internal symmetry of the two-spin state, i.e. an anisotropic term like ΔA in (51) is to be presented in the system Hamiltonian. It is worth mentioning that the idea of using time unitary evolution to measure a symplectic tomography of Bose-Einstein condensate was successfully applied in the paper [52].

8 Conclusions

To conclude we point out the main results of our work.

We applied the tomographic probability approach to the problem of muon spin rotation/relaxation/ resonance experiments. The relation between MuSR histogram and muon spin tomogram was established. In view of this, all MuSR experiments can be interpreted as measuring the reduced tomogram of a quantum state of two-spin system, namely, muon-electron one. The density matrix of this system was mapped onto a joint probability distribution of muon and electron spin projections onto their quantization directions. Such a tomogram was shown to completely describe any muon-electron quantum state. The reduced density matrix describing the muon state was mapped bijectively onto a spin-tomographic probability distribution of the muon spin projection onto a chosen direction (muon spin tomogram).

Time evolution of muon-electron system was investigated within the framework of the tomographic representation. The entanglement phenomenon between muon and electron spins was shown to appear due to different interactions including the hyperfine interaction, the anisotropic hyperfine interaction and the interaction of muon and electron magnetic moments with an external magnetic field. We studied the behavior of the Bell-like tomographic inequality and showed that, for a discussed initial system state, there is no violation of this inequality. The PPT criterion of separability was discussed in the tomographic probability representation. The negativity indicator of entanglement was applied to the muon-electron system. Using such a tomographic entanglement measure, we studied the influence of different kinds of the discussed interactions onto the entanglement phenomenon. The detailed analysis of entanglement under the influence of dissipation within the framework of kinetic equation with relaxation terms is a problem for further consideration.

Acknowledgments

The authors thank the Ministry of Education and Science of the Russian Federation and the Federal Education Agency for support under Project No. 2.1.1/5909 and Contract No. П558 "Application of MuSR method to the investigation of nanostructures." S.N.F. and V.I.M. are grateful to the Russian Foundation for Basic Research for partial support under Projects Nos. 09-02-00142 and 10-02-00312. The authors thank Igor Chernousov for interesting comments.

References

[1] L. D. Landau, *Ztschr. Physik*, **45**, 430 (1927).

[2] J. von Neumann, *Göttingen. Nachr.*, 245 (1927).

[3] U. Fano, *Rev. Mod. Phys.*, **29**, 74 (1957).

[4] E. P. Wigner, *Phys. Rev.*, **40**, 749 (1932).

[5] K. Husimi, *Proc. Phys. Math. Soc. Jpn*, **22**, 264 (1940).

[6] E. C. G. Sudarshan, *Phys. Rev. Lett.*, **10**, 177 (1963).

[7] R. J. Glauber, *Phys. Rev. Lett.*, **10**, 84 (1963).

[8] A. Vourdas, *J. Phys. A: Math. Gen.*, **39**, R65 (2006).

[9] J. Bertrand and P. Bertrand, *Found. Phys.*, **17**, 397 (1987).

[10] K. Vogel and H. Risken, *Phys. Rev. A*, **40**, 2847 (1989).

[11] S. Mancini, V. I. Man'ko, and P. Tombesi, *Quantum Semiclass. Opt.*, **7**, 615 (1995).

[12] D. T. Smithey, M. Beck, M. G. Raymer, and A. Faridani, *Phys. Rev. Lett.*, **70**, 1244 (1993).

[13] J. Mlynek, *Phys. Rev. Lett.*, **77**, 2933 (1996).

[14] J. Radon, *Ber. Verh. Saechs. Akad. Wiss. Leipzig, Math.-Phys. Kl.*, **69**, 262 (1917).

[15] I. M. Gel'fand and G. E. Shilov, *Generalized Functions: Properties and Operations*, Academic Press, New York (1966), Vol. 5.

[16] S. Mancini, V. I. Man'ko, and P. Tombesi, *Phys. Lett. A*, **213**, 1 (1996).

[17] S. Mancini, V. I. Man'ko, and P. Tombesi, *Found. Phys.*, **27**, 801 (1997).

[18] S. Mancini, P. Tombesi, and V. I. Man'ko, *Europhys. Lett.*, **37**, 79 (1997).

[19] K. Banaszek and K. Wodkiewicz, *Phys. Rev. Lett.*, **76**, 4344 (1996).

[20] S. Wallentowitz and W. Vogel, *Phys. Rev. A*, **53**, 4528 (1996).

[21] M. Asorey, P. Facchi, V. I. Man'ko, et al., *Phys. Rev. A*, **77**, 042115 (2008).

[22] M. Asorey, P. Facchi, G. Florio, et al, "Robustness of raw quantum tomography," Los Alamos Arxiv, quant-ph/1003.1664 (2010).

[23] V. V. Dodonov and V. I. Man'ko, *Phys. Lett. A*, **229**, 335 (1997).

[24] V. I. Man'ko and O. V. Man'ko, *J. Exp. Theor. Phys.*, **85**, 430 (1997).

[25] S. N. Filippov and V. I. Man'ko, *J. Russ. Laser Res.*, **30**, 129 (2009).

[26] S. N. Filippov and V. I. Man'ko, *J. Russ. Laser Res.*, **30**, 224 (2009).

[27] V. I. Man'ko, G. Marmo, E. C. G. Sudarshan, and F. Zaccaria, *Phys. Lett. A*, **327**, 353 (2004).

[28] S. N. Filippov and V. I. Man'ko, *J. Russ. Laser Res.*, **31**, 32 (2010).

[29] A. Ibort, V. I. Man'ko, G. Marmo, et al., *Phys. Scr.*, **79**, 065013 (2009).

[30] V. P. Smilga and Yu. M. Belousov, *Muon Metod for Matter Studying*, Nauka, Moscow (1991) [in Russian].

[31] Yu. M. Belousov, V. N. Gorelkin, A. L. Mikaelyan, et. al., *Sov. Phys. Usp.*, **22**, 679 (1979).

[32] Yu. M. Belousov, V. N. Gorbunov, V. P. Smilga, and V. I. Fesenko, *Sov. Phys. Usp.*, **33**, 911 (1990).

[33] C. J. Rhodes, *Annu. Rep. Prog. Chem., Sect. C*, **97**, 315 (2001).

[34] O. Castaños, R. López-Peña, M. A. Man'ko, and V. I. Man'ko, *J. Phys. A: Math. Gen.*, **36**, 4677 (2003).

[35] T. N. Mamedov, V. N. Duginov, V. G. Grebinnik, et. al., *Hyperfine Interactions*, **86**, 717 (1994).

[36] A. S. Baturin and V. N. Gorelkin, *Physica B*, **289–290**, 578 (2000).

[37] V. N. Gorelkin, T. N. Mamedov, A. S. Baturin, *Physica B*, **289–290**, 585 (2000).

[38] V. N. Gorelkin, V. R. Soloviev, A. M. Konchakov, and A. S. Baturin *Physica B*, **289–290**, 409 (2000).

[39] P. Bakule and E. Morenzoni, *Contemporary Physics*, **45**, 203 (2004).

[40] E. Morenzoni, R. Khasanov, H. Luetkens, et. al., *Journal of Neutron Research*, **14**, 269 (2006).

[41] E. Morenzoni, *Physica B*, **404**, 577 (2009).

[42] R. F. Kiefl, M. D. Hossain, B. M. Wojek, et. al., *Phys. Rev. B*, **81**, 180502(R) (2010).

[43] V. A. Andreev and V. I. Manko, *J. Exp. Theor. Phys.*, **87**, 239 (1998).

[44] G. M. D'Ariano, L. Maccone, and M. Paini, *J. Opt. B: Quantum Semiclass. Opt.*, **5**, 77 (2003).

[45] V. N. Chernega and V. I. Man'ko, *J. Russ. Laser Res.*, **28**, 2 (2007).

[46] A. Peres, *Phys. Rev. Lett.*, **77**, 1413 (1996).

[47] M. Horodecki, P. Horodecki, and R. Horodecki, *Phys. Lett. A*, **223**, 1 (1996).

[48] S. N. Filippov and V. I. Man'ko, *J. Russ. Laser Res.*, **29**, 564 (2008).

[49] B. D. Patterson, *Hyperfine Interactions*, **6**, 155 (1979).

[50] B. D. Patterson, *Rev. Mod. Phys.*, **60**, 69 (1988).

[51] A. S. Baturin, V. N. Gorelkin, and R. Singh, *Optics and Spectroscopy*, **94**, 895 (2003).

[52] A. del Campo, V. I. Man'ko, and G. Marmo, *Phys. Rev. A*, **78**, 025602 (2008).